EPI International Journal of Engineering
Volume 5, Number 2, August 2022, pp. 110-116
DOI: 10.25042/epi-ije.082022.06

*p*ISSN 2615-5109
*e*ISSN 2621-0541

Energy-Saving Driving for a Flexible Manipulator by Utilizing Micro Fiber Composite

Akira Abe[a,*]

[a]Department of Systems, Control and Information Engineering, National Institute of Technology, Asahikawa College.
Email: abe@asahikawa-nct.ac.jp

Abstract

In this paper, we examine a point-to-point motion task of a flexible manipulator with macro fiber composite (MFC) and then propose a new feedforward control method to suppress driving energy and residual vibration simultaneously. For this, we use an MFC attached to one side of the flexible manipulator that has one revolute joint as an actuator. We attempt to express the joint angle in the control technique by combining cycloidal and polynomial functions. On the other hand, the input voltage profile of the MFC is expressed using Gaussian functions. The trajectory of the joint angle and the input voltage profile are dependent upon the coefficients of the polynomial function and the Gaussian functions, respectively. The trajectory and the input voltage profile are optimized simultaneously to cancel the residual vibration under saving energy by tuning the coefficients using the particle swarm optimization algorithm. The effectiveness of the proposed method is verified by performing simulations and experiments. Thus, our findings confirmed that the simultaneous optimization of the trajectory of the joint angle and the input voltage of the MFC saves more energy than only the optimization of the trajectory. Therefore, we could establish an energy-saving feedforward control method by driving two actuators.

Keywords: Feedforward control; residual vibration suppression; energy saving; macro fiber composite actuator

1. Introduction

Lighter structures are generally preferred in industrial machinery, from the viewpoint of high-speed operations to improve production efficiency. In particular, there is an increased demand for such structures for robotic manipulators, which are key components of industrial robot systems. A low-stiffness manipulator induces undesirable vibrations, adversely affecting the accuracy of robotic operations. From this perspective, numerous studies [1]–[6] have focused on the vibration control of low-rigidity robot manipulators, treating them as flexible manipulators. In recent years, vibration control of thin-walled structures using piezoelectric elements as actuators has gained much research attention [7]–[12]. Specifically, macro fiber composite (MFC), which is a piezoelectric element, is more suitable for vibration control of flexible structures due to its flexibility, durability, and higher power compared to conventional piezoelectric ceramic PZT. Some researchers have investigated the vibration control of flexible manipulators using MFC as actuators. For example, Yang et al. [13] investigated the dynamic modeling and adaptive vibration suppression of a flexible macro-micro manipulator, which comprised a macro stage and a flexible MFC micromanipulator. They considered a nonlinearity of the MFC based on the Bouc–Wen hysteresis equation in dynamic modeling. They also presented a hybrid control strategy consisting of a trajectory planning method of the joint angle of the macro stage and an adaptive variable structure control by the MFC actuator to simultaneously suppress the vibration during and after the positioning. Wang et al. [14] proposed a robust vibration control technique for the MFC micromanipulator based on a macro stage in translational motion. They employed an asymmetric Prandtl–Ishlinskii hysteresis model in their proposed technique to capture the hysteresis nonlinearity of an MFC. They also adopted a perturbation H-infinity controller to compensate for structural uncertainty. Feng et al. [15] developed a model-independent adaptive fuzzy controller (AFC) for suppressing the vibrations of a two-link flexible manipulator system, where a pair of MFC actuators were attached to the root of each flexible link. They also demonstrated the effectiveness of the control performance of the proposed AFC using both simulations and experiments.

However, most of the studies of flexible manipulators have focused only on vibration suppression, and there is a lack of sufficient research on feedforward vibration control that is compatible with energy conservation. Thus, the present authors [16]–[18] have studied the point-to-point (PTP) control problem of mechanical systems consisting of flexible links and have proposed feedforward vibration control methods that simultaneously minimize the driving energy and residual vibration. A previous study

*Corresponding author.
Shunkodai 2-2-1-6
Asahikawa, Hokkaido, Japan
071-8142

[19] established a trajectory planning method for flexible robotic manipulators using a combination of cycloidal and polynomial functions to minimize residual vibration and operating energy simultaneously. The findings of our previous research indicated that the energy saving of flexible manipulators could be further enhanced by actively utilizing their inherent flexibility. Therefore, this paper investigates the feedforward vibration control method of a flexible manipulator with an MFC actuator, and then inquires the possibility of further energy savings from the interaction of the two actuators, a servo motor and the MFC. This paper contributes to presenting a novel energy-saving feedforward control technique for a flexible manipulator by utilizing MFC as an actuator.

2. Experimental Setup and Mathematical Model

The dimensions of the flexible manipulator treated in this study are shown in Fig. 1. A brass beam measuring 510 mm (length, l) × 65 mm (width, b) × 1 mm (thickness, h) is used as the flexible manipulator, and a piezoelectric device is attached to one side of the manipulator at 16 mm from the fixed end. An MFC (M-8557-P1) is used as the piezoelectric device, and its input voltage ranges from −500 to 1500 V.

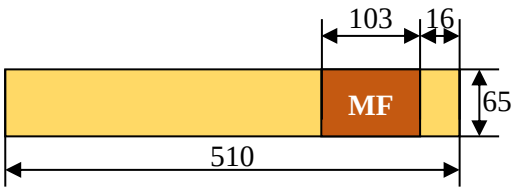

Figure 1. Schematic sketch of the flexible manipulator

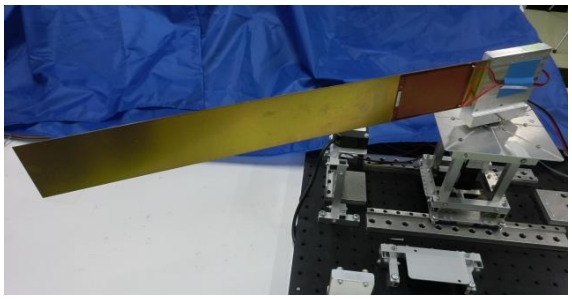

Figure 2. Photograph of the experimental setup

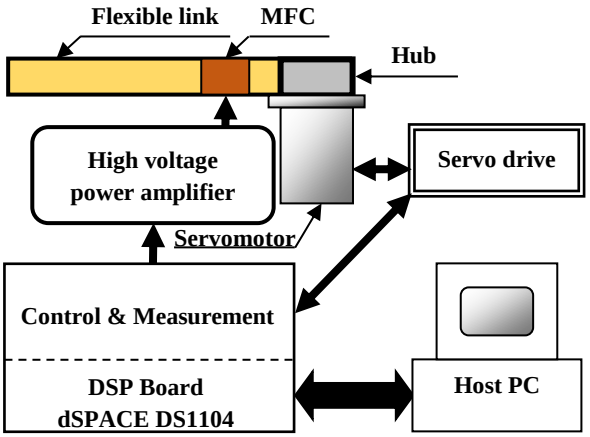

Figure 3. Schematic diagram of the experimental setup

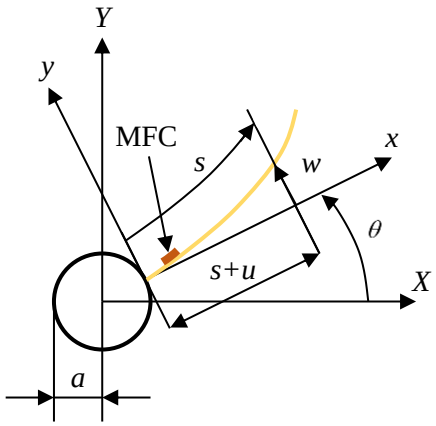

Figure 4. Coordinate systems of flexible manipulator

A photograph and schematic diagram of the experimental setup are shown in Figs. 2 and 3, respectively. Figure 4 depicts the coordinate systems of the flexible manipulator, where the radius of the rigid hub (45 mm) is denoted by a. The joint angle θ of the flexible link is actuated by an AC servomotor (YASKAWA: SGMMJ-A3EAAJ361K), which is operated in the speed control mode using a servo drive (YASKAWA: SGDJ-A3ESY32). The displacement w of the flexible manipulator is measured by attaching a strain gauge to the opposite side of the MFC. The motor torque τ is monitored using the servo drive. The MFC is driven using a power amplifier (TREK: MODEL 2220) for piezo actuators, and its drive voltage is measured from the analog monitor function of the power amplifier. Measurement and control of the experimental setup are implemented on a DSP board (dSPACE: DS1104), which has a sampling rate of 500 Hz. As shown in Fig. 4, the MFC is attached to the upper surface of the manipulator and is stretched since the displacement w is positive upward y. Consequently, the manipulator is deformed in the negative direction when a positive voltage is applied.

Based on the modeling of flexible manipulators in a previous study [16], we assume that the equations of motion are as follows:

$$\ddot{W} + 2\varsigma\omega\dot{W} + \omega^2 W + \alpha_1\ddot{\theta} + \alpha_2\dot{\theta}^2 W = -\alpha_3 u \tag{1}$$

$$\beta_1\ddot{\theta} + \beta_2\ddot{W} + c_\theta\dot{\theta} = \tau \tag{2}$$

where W denotes the modal amplitude of the first vibration mode, u denotes the control input from the MFC, and ζ and c_θ denote the viscous damping and friction coefficients, respectively. A dot denotes the derivative with respect to time t. Note that the flexible manipulator is approximated as a uniform beam because the thickness of the MFC is very thin (0.3 mm). The characteristic of the MFC is approximated by the following first-order system

$$\dot{u} = \beta u + v \tag{3}$$

where v denotes the input voltage of the MFC.

Table 1. Identified parameters

Parameter	Value	Unit
α_1	2.708×10^{-1}	m
α_2	2.176×10^{-1}	-
α_3	3.062×10^{-2}	m/(Vs^3)
ζ	1.366×10^{-2}	-
β_1	2.232×10^{-2}	kgm^2
β_2	8.258×10^{-2}	kgm
c_θ	2.989×10^{-2}	Nms/rad
β	−83.23	1/s

Since the proposed method belongs to a feedforward controller, its performance depends on the accuracy of the controlled object. Thus, the values of the coefficients in equations (1)-(3) are determined from parameter identification experiments in order to obtain an accurate mathematical model [18]–[20]. These values are determined in the identification technique so that the simulation and experimental results are in good agreement with each other. The obtained values are listed in Table 1. The validity of the values will be shown by experimental results in a later section.

3. Feedforward Control Method

In this section, we deal with the PTP motion of the flexible manipulator and present a feedforward control technique for suppressing residual vibrations with minimum driving energy consumption.

We attempt to express the joint angle profile of the flexible manipulator as the following cycloidal function [19]

$$\theta(t) = \theta_E \left\{ U(t) - \frac{\sin[2\pi U(t)]}{2\pi} \right\}, \quad t \in [0, T_E] \tag{4}$$

where θ_E and T_E denote the target angle and traveling time of the PTP motion, respectively. The input function $U(t)$ of the cycloidal function is defined as [19]

$$U(t) = \frac{t}{T_E} + (1 - T^2) \sum_{m=1}^{M} a_m T^{m-1} \tag{5}$$

where

$$T = -1 + \frac{2t}{T_E} \tag{6}$$

The input voltage profile of the MFC is represented by using a Gaussian function:

$$v(t) = (1 - T^2) d \exp\left[-\frac{(T - c)^2}{\sigma^2} \right], \quad t \in [0, T_E] \tag{7}$$

where the definition of T is the same as in Eq. (6). Figure 5 indicates the output of Eq. (7) in a graph when $T_E = 1$, $d > 0$, $c = -1$, and $\sigma^2 = 0.1$, in which the maximum value is normalized to 1. As shown in Fig. 5, the Gaussian function outputs a pulse-like waveform, whose voltage we will attempt to apply to the MFC in this study. The parameter c in Eq. (7) is set to $c = -3$. The value of the parameter d is adopted so that the maximum value of v is 1000 V.

The trajectory $\theta(t)$ and the input voltage profile $v(t)$ depend on the coefficients a_m in Eq. (5) and σ in Eq. (7), respectively. Hence, the coefficients need to be tuned in order to suppress the residual vibration under the saving energy. An overview of the parameter tuning method is given below.

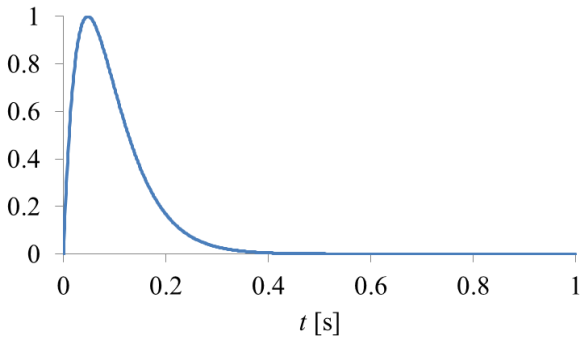

Figure 5. Shape of the Gaussian function

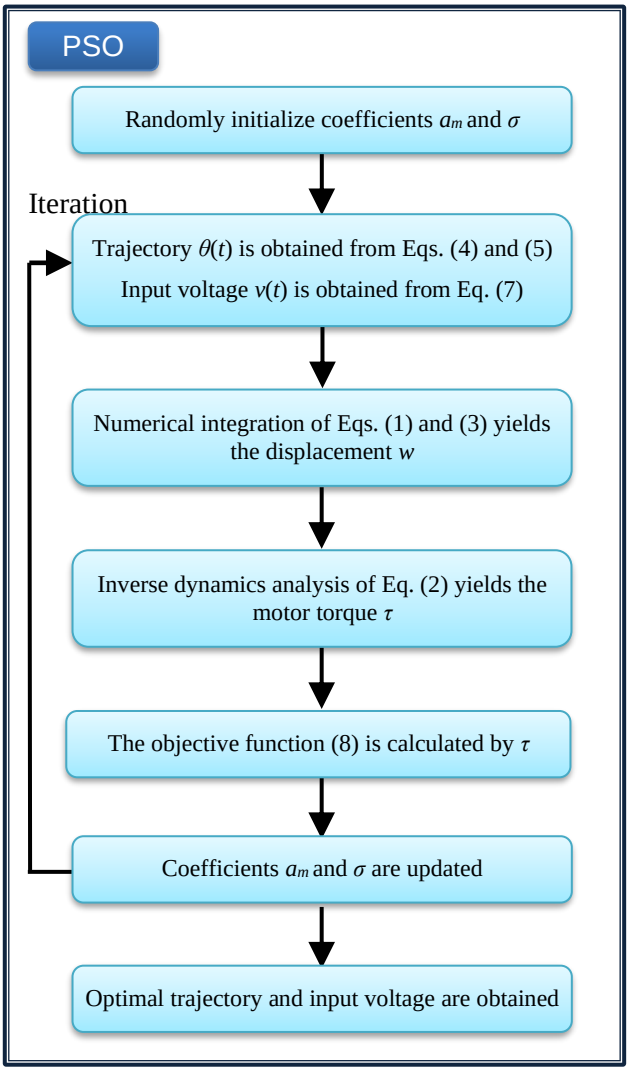

Figure 6. Schematic algorithm of the proposed method

Figure 6 shows the algorithm of the proposed method. First, we give a driving condition (θ_E and T_E). The coefficients a_m and σ are set as optimization parameters, and then we generate the trajectory $\theta(t)$ and the input voltage profile v(t) from Eqs. (4), (5), and (7). The numerical integrations of Eqs. (1) and (3) yield the displacement w of the flexible manipulator. We then determine the motor torque τ from the inverse dynamics analysis of Eq. (2) using the obtained accelerations $\ddot{\theta}$ and $\ddot{w}$. To simultaneously minimize the residual vibration and driving energy, we define the objective function F as follows [21]:

$$F = F_1 + F_2 = \sum_{i=1}^{I} |\tau_i| + \sum_{i=I+1}^{I+J} |\tau_i| \tag{8}$$

where τ_i denotes the torque at sampling time Δt = 2 ms and $I = (T_E+1)/\Delta t$. The function F_1 denotes the total sum of the torques until the positioning of the PTP motion. The function F_2 represents the sum of the torque for 1 s after the positioning, where $J = 1/\Delta t$. Minimization of F_1 and F_2 can suppress the driving energy and the residual vibration, respectively. The particle swarm optimization (PSO) algorithm [22] tunes the optimized parameters to minimize the objective function (8). Finally, the optimal trajectory and input voltage are obtained. Note that the residual vibration can be suppressed with energy savings when the flexible manipulator is driven using optimal trajectory and input voltage, and the proposed method belongs to the feedforward vibration control scheme.

4. Simulation and Experimental Results

Numerical simulations and experiments are performed to verify the validity of the proposed energy-saving feedforward vibration control method. The below simulations involve 50 particles and 400 iterations (maximum) in the PSO algorithm. The number of terms in Eq. (5) is adopted as M = 6, and the ranges of the optimization parameters are defined as

$$\left.\begin{aligned} a_m &\in [-0.2, 0.2], (m = 1, 2, \cdots, 6) \\ \sigma^2 &= 10^{-q}, q \in [-1, 0] \end{aligned}\right\} \tag{9}$$

Figure 7 shows a comparison of the simulation results obtained by the present method and a cycloidal motion, in which the driving condition is set as $\theta_E = -\pi/4$ rad and T_E = 1.0 s. The cycloid motion is obtained as $U(t) = t/T_E$ in Eq. (4). Here, note that the MFC is not driven for the results of the cycloid motion. The time histories of the joint angle, angular velocity, tip displacement, input voltage, and motor torque are depicted in Figs. 7 (a)–(e), respectively. The cycloidal motion induces the residual vibration after the positioning (t > 1 s), and this residual vibration causes torque to keep the joint angle at the target angle θ_E, as shown in Fig. 7 (e). After the positioning, the vibration and torque are perfectly canceled in the present method. Thus, this indicates that the proposed method, which is based on minimizing the drive torque defined in Eq (8), can suppress the residual vibration.

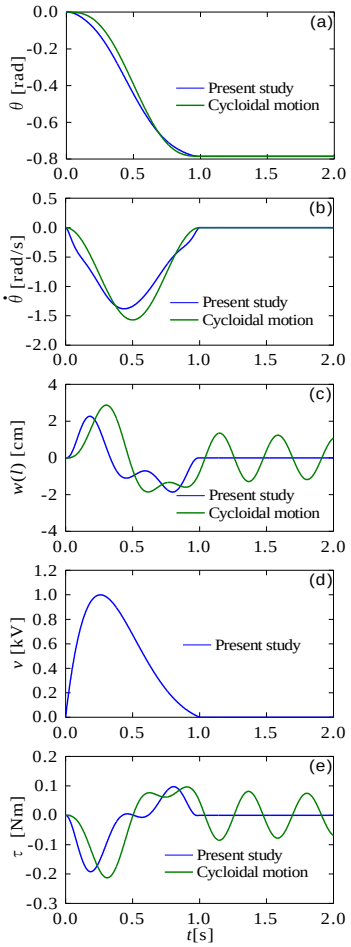

Figure 7. Comparison of simulation results obtained using the present method and a cycloidal motion (T_E = 1.0 s and $\theta_E = -\pi/4$ rad): (a) joint angle, (b) angular velocity, (c) tip displacement, (d) input voltage, and (e) motor torque

Figure 8 illustrates a comparison of the simulation and experimental results obtained by the present method, where the driving conditions are the same as in Fig. 7. As shown in the figure, the simulation and experimental results are in good agreement with each other, thus validating the modeling of the flexible manipulator with the MFC. As shown in Fig. 8 (b) that depicts the time history of tip displacement, the proposed method also suppresses the residual vibration in the experiment. This confirms the effectiveness and feasibility of the feedforward vibration control technique through the simultaneous optimization of the two actuators. For comparison, the results obtained by the previous study [19], in which the trajectory of the joint angle is only optimized without using the MFC, are shown in Fig. 9. As shown in this figure, residual vibration suppression can be achieved in both simulation and experiment. Figure 10 presents a comparison of the simulation results obtained by the present and previous studies shown in Figs. 8 and 9, respectively. Figures 10 (a) and 10 (b) indicate tip displacement and motor torque, respectively. As shown in Fig. 10 (a), the maximum value of displacement at t = 0.18 s in the present study is less than that in the previous study [19]. This reduction in the maximum displacement is caused by MFC actuation whose input voltage has a peak at around t = 0.25 s as shown in Fig. 8 (d). Due to this

deformation suppression effect, the maximum value of the torque is also slightly lower in the present method than in the previous study [19].

Regarding the energy-saving effect of the present method, Table 2 shows a comparison of the driving energy calculated by the experimental data under three driving conditions ($\theta_E = -\pi/4$ rad and $T_E = 0.9$ s), ($\theta_E = -\pi/4$ rad and $T_E = 1.0$ s), and ($\theta_E = -\pi/2$ rad and $T_E = 1.1$ s). The values in parentheses are obtained from the simulation results. The driving energy *Ene* is defined as follows:

$$Ene = \int_0^{\theta_E} |\tau| \, d\theta \tag{10}$$

The vibration control performance of both methods was also checked under driving conditions ($\theta_E = -\pi/4$ rad and $T_E = 0.9$ s) and ($\theta_E = -\pi/2$ rad and $T_E = 1.1$ s). The time history data comparing simulation results with experimental results are presented in the Appendix. The experimental results tend to have larger values than the simulation results probably due to the frictions of the motor, which are not considered in the mathematical model. As demonstrated in Table 2, under all drive conditions, the values for the present method are smaller than those for the previous method, and the energy-saving effect of the proposed method can be confirmed by actuating the MFC. On the other hand, the driving energy of the MFC is not considered, as shown in Eq. (10). Figure 11 shows the displacement obtained from the simulation when the joint angle of the manipulator is fixed, and the input voltage shown in Fig. 7 (d) is applied to the MFC. By using this displacement data, the driving energy of the MFC can be calculated from the maximum potential energy as follows:

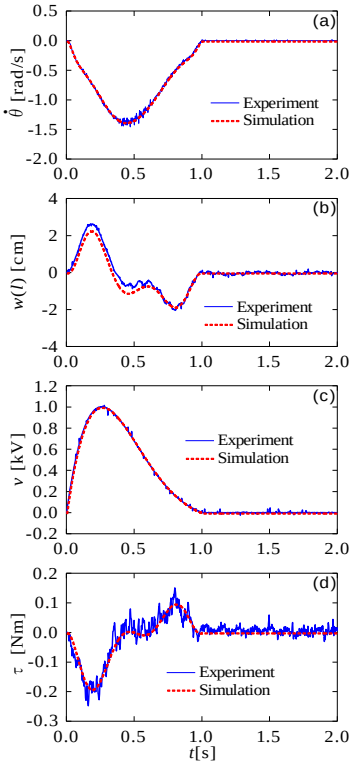

Figure 8. Comparison of simulation and experimental results obtained using the present method ($T_E = 1.0$ s and $\theta_E = -\pi/4$ rad): (a) angular velocity, (b) tip displacement, (c) input voltage, and (d) motor torque

$$U_{\max} = \max\left[\frac{EI}{2}\int_0^l \left(\frac{\partial^2 w}{\partial s^2}\right)^2\right] \tag{11}$$

where *EI* represents the flexural rigidity of the flexible manipulator. Note that the maximum amplitude of the tip displacement is only about 0.8 cm and the calculated energy of the MFC is about 1×10^{-4} J, which is significantly less than that of the motor and can be ignored. Therefore, this finding shows that the proposed method enables further energy savings under residual vibration suppression.

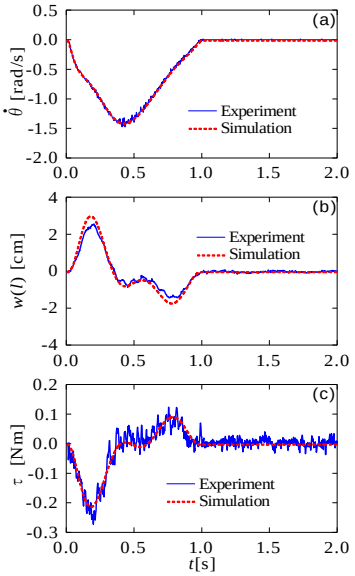

Figure 9. Comparison of simulation and experimental results obtained using the previous method ($T_E = 1.0$ s and $\theta_E = -\pi/4$ rad): (a) angular velocity, (b) tip displacement, and (c) motor torque

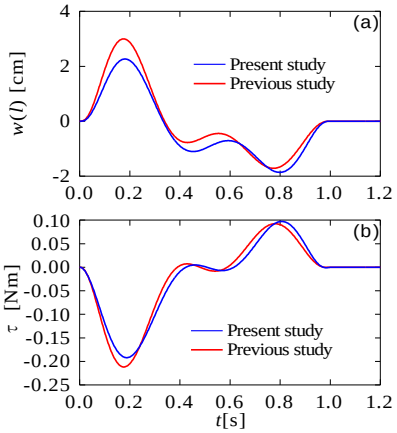

Figure 10. Comparison of simulation results obtained using the present method and the previous method ($T_E = 1.0$ s and $\theta_E = -\pi/4$ rad): (a) tip displacement and (b) motor torque

Table 2. Comparison of driving energy *Ene* [J]

θ_E [rad]	T_E [s]	Present study	Previous study [19]
$-\pi/4$	0.9	5.85×10^{-2} (5.28×10^{-2})	6.23×10^{-2} (5.64×10^{-2})
$-\pi/4$	1.0	5.09×10^{-2} (4.41×10^{-2})	5.35×10^{-2} (4.63×10^{-2})
$-\pi/2$	1.1	1.60×10^{-1} (1.53×10^{-1})	1.73×10^{-1} (1.64×10^{-1})

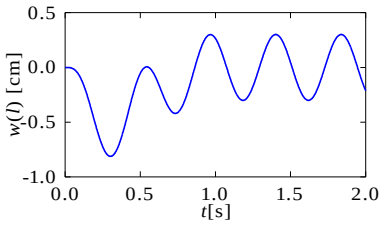

Figure 11. Tip displacement calculated using the input voltage of MFC shown in Fig. 7 (d) when the joint angle is fixed

5. Summary

This study examined the PTP control problem of a flexible manipulator that consists of two actuators, a servo motor and MFC, and proposed a novel energy-saving feedforward control technique. Simulation and experimental results revealed that simultaneous optimization of the input voltage of MFC and the trajectory of the joint angle is more energy-saving than only optimization of the trajectory of the joint angle. To the best of our knowledge, this study presents a novel finding that the driving energy of a flexible manipulator can be reduced by utilizing deflection due to an MFC during a PTP motion.

References

[1] M. Benosman and G. L. Vey, "Control of flexible manipulators: A survey," *Robotica*, vol. 22, no. 5, pp. 533–545, 2004.

[2] S. K. Dwivedy and P. Eberhard, "Dynamic analysis of flexible manipulators, a literature review," *Mech. Mach. Theory*, vol. 41, no. 7, pp. 749–777, 2006.

[3] H. N. Rahimi and M. Nazemizadeh, "Dynamic Analysis and Intelligent Control Techniques for Flexible Manipulators: A Review," *Adv. Robot.*, vol. 28, no. 2, pp. 63–76, 2014.

[4] C. T. Kiang, A. Spowage, and C. K. Yoong, "Review of Control and Sensor System of Flexible Manipulator," *J. Intell. Robot. Syst.*, vol. 77, no. 1, pp. 187–213, 2015.

[5] K. Lochan, B. K. Roy, and B. Subudhi, "A Review on Two-Link Flexible Manipulators," *Annu. Rev. Control*, vol. 42, pp. 346–367, 2016.

[6] E. A. Alandoli and T. Lee, "A Critical Review of Control Techniques for Flexible and Rigid Link Manipulators," *Robotica*, vol. 38, no. 12, pp. 2239–2265, 2020.

[7] R. Rimašauskienė, V. Jūrėnas, M. Radzienski, M. Rimašauskas, and W. Ostachowicz, "Experimental analysis of active–passive vibration control on thin-walled composite beam," *Compos. Struct.*, vol. 223, p. Article 110975, 2019.

[8] J. Gawryluk, A. Mitura, and A. Teter, "Dynamic control of kinematically excited laminated, thin-walled beam using macro fibre composite actuator," *Compos. Struct.*, vol. 236, p. Article 111898, 2020.

[9] X. Wanga, W. Zhoub, Z. Zhanga, Jianga, and Z. Wu, "Theoretical and Experimental Investigations on Modified LQ Terminal Control Scheme of Piezo-Actuated Compliant Structures in Finite Time," *J. Sound Vib.*, vol. 491, p. Article 115762, 2021.

[10] J. Zhou, J. Zhou, W. Chen, J. Tian, J. Shen, and P. Zhang, "Macro Fiber Composite-Based Active and Efficient Suppression of Low-Frequency Vibration of Thin-Walled Composite Beam," *Compos. Struct.*, vol. 299, p. Article 116019, 2022.

[11] G. Zhiyuan, W. Yiru, S. Muyao, and Z. Xiaojin, "Theoretical and Experimental Investigation Study of Discrete Time Rate-Dependent Hysteresis Modeling and Adaptive Vibration Control for Smart Flexible Beam with MFC Actuators," *Sensors Actuators A Phys.*, vol. 344, p. Article 109332, 2022.

[12] Q. Lu, P. Wang, and C. Liu, "An Analytical and Experimental Study on Adaptive Active Vibration Control of Sandwich Beam," *Int. J. Mech. Sci.*, vol. 232, p. Article 107634, 2022.

[13] Y. L. Yang, Y. D. Wei, J. Q. Lou, L. Fu, S. Fang, and T. H. Chen, "Dynamic Modeling and Adaptive Vibration Suppression of a High-Speed Macro-Micro Manipulator," *J. Sound Vib.*, vol. 422, pp. 318–342, 2018.

[14] S. Wang, Y. L. Yang, G. P. Li, H. L. Du, and Y. D. Wei, "Microscopic Vibration Suppression for a High-Speed Macro-Micro Manipulator with Parameter Perturbation," *Mech. Syst. Signal Process.*, vol. 179, p. Article 109332, 2022.

[15] C. Feng, W. Chen, M. Shao, and S. Ni, "Trajectory Tracking and Adaptive Fuzzy Vibration Control of Multilink Space Manipulators with Experimental Validation," *Actuators*, vol. 12, p. 138, 2023.

[16] A. Abe and K. Komuro, "Minimum Energy Trajectory Planning for Vibration Control of a Flexible Manipulator Using a Multi-Objective Optimization Approach," *Int. J. Mechatronics Autom.*, vol. 2, no. 4, pp. 286–294, 2012.

[17] A. Abe and S. Nemoto, "An Energy Saving Feedforward Control Technique for a 2-DOF Flexible Manipulator (in Japanese)," *Trans. Japan Soc. Mech. Eng. Ser. C*, vol. 78, pp. 1325–1337, 2012.

[18] A. Abe, "Minimum Energy Trajectory Planning Method for Robot Manipulator Mounted on Flexible Base," in *Proceeding of 9th Asian Control Conference*, 2013, pp. 1–7.

[19] A. Abe, "An Effective Trajectory Planning Method for Simultaneously Suppressing Residual Vibration and Energy Consumption of Flexible Structures," *Case Stud. Mech. Syst. Signal Process.*, vol. 4, pp. 19–27, 2016.

[20] A. Abe, "Trajectory Planning for Flexible Cartesian Robot Manipulator by Using Artificial Neural Network: Numerical Simulation and Experimental Verification," *Robotica*, vol. 29, no. 05, pp. 797–804, 2011.

[21] A. Abe, "Trajectory Panning of a Flexible Manipulator Based on Driving Torque (in Japanese)," *Trans. Japan Soc. Mech. Eng. Ser. C*, vol. 74, pp. 2246–2253, 2008.

[22] M. Clerc and J. Kennedy, "The Particle Swarm-Explosion, Stability, and Convergence in a Multidimensional Complex Space," *IEEE Trans. Evol. Comput.*, vol. 6, no. 1, pp. 58–73, 2002.

Appendix A. Experimental validation

Figures A1–A4 present a comparison of simulation and experimental results obtained using the present and previous methods under the driving conditions ($\theta_E = -\pi/4$ rad and $T_E = 0.9$ s) and ($\theta_E = -\pi/2$ rad and $T_E = 1.1$ s). As shown in Figs. A1–A4, the experimental results are in good agreement with the simulation results. We also demonstrate that the proposed feedforward vibration control technique is effective and feasible.

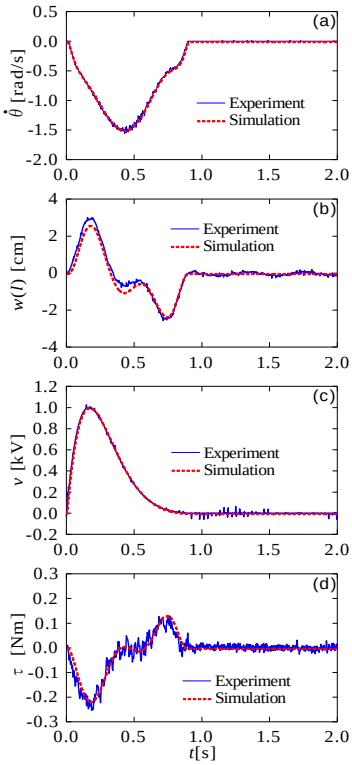

Figure A1. Comparison of simulation and experimental results obtained using the present method (T_E = 0.9 s and θ_E = −π/4 rad): (a) angular velocity, (b) tip displacement, (c) input voltage, and (d) motor torque.

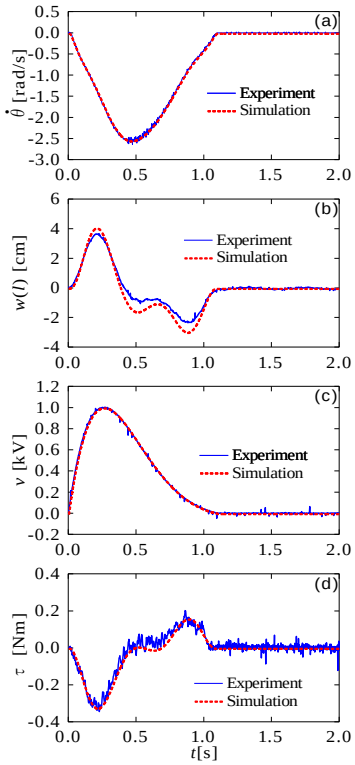

\Fig. A3 Comparison of simulation and experimental results obtained using the present method (T_E = 1.1 s and θ_E = −π/2 rad): (a) angular velocity, (b) tip displacement, (c) input voltage, and (d) motor torque.

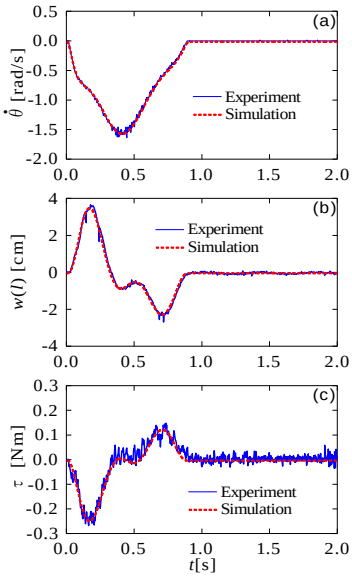

Fig. A2 Comparison of simulation and experimental results obtained using the previous method (T_E = 0.9 s and θ_E = −π/4 rad): (a) angular velocity, (b) tip displacement, and (c) motor torque.

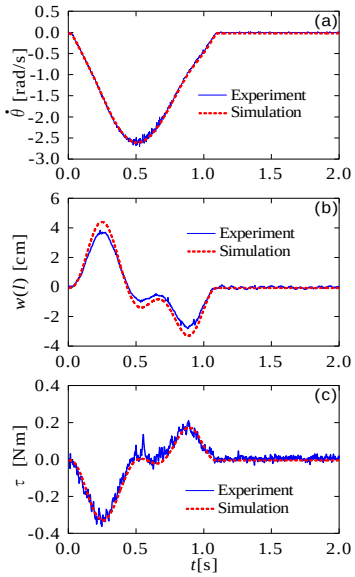

Fig. A4 Comparison of simulation and experimental results obtained using the previous method (T_E = 1.1 s and θ_E = −π/2 rad): (a) angular velocity, (b) tip displacement, and (c) motor torque.